Nucleation and Crystal Growth Kinetics of Strengite, FePO$_4$,2H$_2$O, in Aqueous Solution

Hans E. Lundager Madsen and Christian Bender Koch

Affiliation:
Chemistry Department, University of Copenhagen, Universitetsparken 5, DK-2100 Copenhagen, Denmark

Correspondence addresses: helm@chem.ku.dk, cbk@chem.ku.dk

Abstract

Crystallization kinetics of strengite, FePO$_4$,2H$_2$O, has been investigated by direct mixing of ammonium phosphate solution with a solution containing either iron(III) or iron(II) plus hydroxylamine, the latter acting as oxidant on the surface of growing iron phosphate crystals. Nucleation rate was determined by light scattering and crystal growth rate from pH recording. From the former was found a relatively uncertain surface fre energy of 127 mJ/m² with Fe(III) and a much more precise value of 55 mJ/m² with Fe(II) + HONH$_2$. Crystal growth was shown to take place mainly by surface nucleation, either the mononuclear or the polynuclear mechanism, and yielded edge free energies of 86-92 pJ/m with Fe(III) and 13-22 pJ/m with Fe(II) + HONH$_2$. The large differences may be interpreted in terms of a Fe(II)-rich monolayer on crystals growing from solution containing iron(II) and hydroxylamine.

1. Introduction

Two of the more widespread iron phosphates found as minerals are the iron(II) salt vivianite, Fe$_3$(PO$_4$)$_2$,8H$_2$O, and the iron(III) salt strengite, FePO$_4$,2H$_2$O. One or the other is often found together with other iron minerals such as pyrite, goethite and limonite and, of course, other iron phosphates.[1,2] Whether one or the other is abundant at a given location depends on redox conditions at the site, the former preferring anoxic, the latter oxic environments. Strengite is most often found as very small crystals. They belong to the orthorhombic bipyramidal class *mmm*, the main crystallographic parameters being[3]

a = 872.2 pm, b = 987.8 pm, c = 1011.87 pm, Z = 8

According to Groth,[4] the dominating forms are {100}, {111} and {102} (Groth gives the latter form as {120}, because he takes the long axis as *b*).

The original aim of our investigation on iron phosphates was crystallization kinetics of vivianite. It is well known to chemists working with transition metal salts in aqueous solution that Fe^{2+} is easily oxidized, when the solution is in contact with air, resulting in precipitation of iron(III) hydroxide:

$$4\ Fe^{2+} + O_2 + 10\ H_2O \rightarrow 4\ Fe(OH)_3 + 8\ H^+$$

Visible color change as well as beginning precipitation in a solution of an iron(II) salt will typically

be observed already after a few hours, even when the solvent is water purged with nitrogen. In order to avoid the complications of working under a nitrogen atmosphere throughout, we attempted to stabilize the system in oxidation stage II by addition of a suitable reducing agent. Hydroxylammonium chloride was chosen, because this chemical is used to reduce iron(III) in water analyses[5]:

$$4\ Fe^{3+} + 2\ NH_3OH^+ \rightarrow 4\ Fe^{2+} + N_2O + 6\ H^+ + H_2O$$

Despite this precaution, however, the precipitate obtained was not, as expected, vivianite, which forms relatively large and characteristic crystals,[6] but nanocrystals of strengite. In fact, hydroxylamine is not only reducing, but strongly oxidizing as well, the standard potential of the couple $NH_3OH^+|NH_4^+$ being as high as $E^\ominus = 1.35$ V.[7] We infer that the actual process of precipitation in the presence of hydroxylamine is

$$2\ Fe^{2+} + 2\ H_2PO_4^- + NH_3OH^+ + 3\ H_2O \rightarrow 2\ FePO_4,2H_2O + NH_4^+ + 2\ H^+$$

Apparently a growing crystal of iron phosphate somehow catalyzes the process of oxidation. For comparison we also made a series of precipitations directly from iron(III) and phosphate without additive:

$$Fe^{3+} + H_2PO_4^- + 2\ H_2O \rightarrow FePO_4,2H_2O + 2\ H^+$$

Since H^+ is liberated in the process of precipitation both with and without additive, pH recording is a suitable method of measurement. In further experiments nucleation was detected by light scattering (turbidimetry) like in a previous study on calcium fluoride.[8]

2. Materials and methods

2.1. Apparatus

Two different pH meters were used for pH recording. In the first series it was a Radiometer pH/ion meter model PHM 240 with a Metrohm Solitrode combination electrode. It was connected to a serial port of a PC, which stored the readings at suitable time intervals. In the second series a Mettler-Toledo SevenCompact pH meter with an InLab ExpertPro ISM combination electrode was used. With this latter instrument connection to a PC during a kinetic experiment was unnecessary, as the storage capacity of the meter is 1000 measurements. The time interval of measurements is entered into the instrument before start. Values were afterwards transferred to a USB stick and from there into the computer for data processing. Both pH meters were calibrated with ISO standard buffers: potassium tetraoxalate, 0.05 molkg, pH = 1.680, potassium hydrogen phthalate, 0.05 mol/kg, pH = 4.008, potassium dihydrogen phosphate + sodium hydrogen phosphate, both 0.025 mol/kg, pH = 6.865, and borax, 0.01 mol/kg, pH = 9.184, all pH values applying to 25°C.

Turbidity spectra for determination of nucleation rates were recorded with a World Precision Instruments/Ocean Optics model SD2000 fiber optic spectrometer with spectral range 250-850 nm and resolution 1.9 nm. The light source was a World Precision Instruments D_2Lite combined deuterium and tungsten/halogen lamp. Samples were placed in standard 1-cm quartz cuvettes inserted in an Ocean Optics CUV-UV cuvette holder connected to a circulation thermostat.

Precipitate was examined by dark-field microscopy, using a Zeiss Jenapol microscope equipped with a Zeiss cardioid condenser. As this method did not provide a definite identification

of the precipitate as strengite, further studies were made with scanning electron microscopy, x-ray powder diffraction and Mössbauer spectroscopy. Micrographs of uncoated samples were obtained at low vacuum using a FEI FEG microscope. Diffractograms were obtained using a D8 Bruker diffractometer equipped with Cu tube and a Lynx Eye detector. Mössbauer spectra were obtained at room temperature with a Wissel spectrometer calibrated using a natural Fe foil at room temperature. The spectrum was fitted using 2 doublet components with Lorentzian line shape.

2.2. Reagents

Stock solutions for precipitation experiments were diammonium iron(II) sulfate hexahydrate (Mohr's salt) + hydroxylammonium chloride, both 0.1 M, ammonium iron(III) sulfate dodecahydrate (iron alum), 0.1 M, as well as 0.1 M solutions of ammonium dihydrogen phosphate and diammonium hydrogen phosphate. Iron alum was BDH Analar, the other chemicals were Merck p.a. Solvent, also used for dilution, was either Milli-Q water (Millipore Corp.) or demineralized water further purified by passing through a filter with activated carbon and a Silhorko Silex 1 mixed-bed ion exchange column.

2.3. Procedures

Experiments with pH recording were carried out at 25 and 35°C for the systems with iron(II) and hydroxylamine, but only at 25°C with pure iron(III). To a test tube of 20 mL was added 5 mL of a suitable mixture of the two ammonium phosphates; in a number of cases only the dihydrogen phosphate was used. To another test tube was added 5 mL of either iron(II)/hydroxylamine or iron(III) solution. Both test tubes were immersed in a water thermostat. After a few minutes the solutions were mixed in one of the test tubes, the pH electrode inserted, and pH recording started. The initial time interval of storing pH values was 1 minute. With the Radiometer instrument, the program in the computer, to which it was connected, doubled the interval when pH had decreased by less than 0.01 since the previous reading. Recording was stopped when more than 12 hours had elapsed since the start of the experiment. With the Mettler-Toledo instrument the time interval could not be changed during a run, so measurements continued until memory was full, i.e. after nearly 17 hours. Towards the end of an experiment there was very little, if any, variation in pH values, so some data had to be deleted to make the outcome similar to that from the other pH meter. In both cases a final pH reading was taken the following day, and a sample of precipitate was taken for microscopic characterization.

In the recordings of turbidity spectra the program on the PC to which the spectrometer was connected was set to Time Acquisition such as to store the absorbances (turbidities) once a minute at six different wavelengths: 400, 480, 560, 640, 720 and 800 nm. The spectra of the iron stock solutions as recorded on the spectrometer showed no measurable light absorption above 350 nm. The total volume of solution in the cuvette was 3 mL. Recording of spectral data was started as soon as the last reagent solution had been added to the cuvette. After a certain period, which depended on initial supersaturation, absorbance at 400 nm had reached a value of about 2, and then the signal-to-noise ratio at this wavelength was too low to ensure reliable measurement. The experiment was then stopped. All these experiments were made at 25°C.

3. Calculations

Knowing the initial composition of the solution as well as the recorded pH values we may, assuming that only strengite crystallizes and with the aid of literature data for relevant equilibrium constants[9,10,11,12,13] calculate all concentrations, amount of solid precipitated and residual

supersaturation at any time during the process. A previously described computer program,[14,15] recently revised such as to run under Microsoft Windows 10, has been used for these calculations. The rate R of advancement of a crystal face was assumed proportional to the third root of amount precipitated; this is equivalent with the assumption of a constant number of growing crystals during the process. Further calculations on crystal growth rates will be described below in the section Results.

Turbidity data from spectroscopy were evaluated using the Mie theory for light scattering from small particles.[16,17] We have no explicit expression for calculating particle size or number density from turbidity data. Instead, the method is based on the extinction efficiency factor

$$Q_{ext} = \frac{\tau}{\pi N a^2} \tag{1}$$

where τ is the turbidity, corresponding to absorbance in a cuvette of unit length, N is the number of particles per unit volume, and a is the radius of a particle. Q_{ext}, in turn, is a function of a, wavelength λ and the refractive indices of particle and surrounding medium. In the present study Q_{ext} is calculated from these latter parameters using the method of phase angles.[17] For each set of 6 turbidity values at the selected wavelengths recorded at a given time, a is adjusted until the dependence of calculated values of Q_{ext} on λ agrees with the variation of τ with λ. The calculation involves the summation of more than 20 spherical Bessel functions, but with a suitable recursion formula readily implemented in the computer program this is a relatively simple task.[8] Knowing a we obtain N from (1), and the increase of N with time gives the rate of nucleation J.

4. Results

Figure 1 shows at left and center crystals of strengite formed by direct precipitation from iron alum and ammonium phosphate. Images from all other precipitates were similar, including those from iron(II) and hydroxylamine. The crystals are on the average about 0.1 µm across, those from iron(II) and hydroxylamine apparently a little larger. At right is shown for comparison crystals formed by air oxidation of iron(II) in phosphate solution in a test tube covered with Parafilm. This results in slow increase of saturation ratio of strengite and thus a low rate of nucleation, such that much larger crystals are formed than in the case of direct addition of iron(III). In plane polarized light these crystals showed symmetric extinction as expected for orthorhombic crystals.
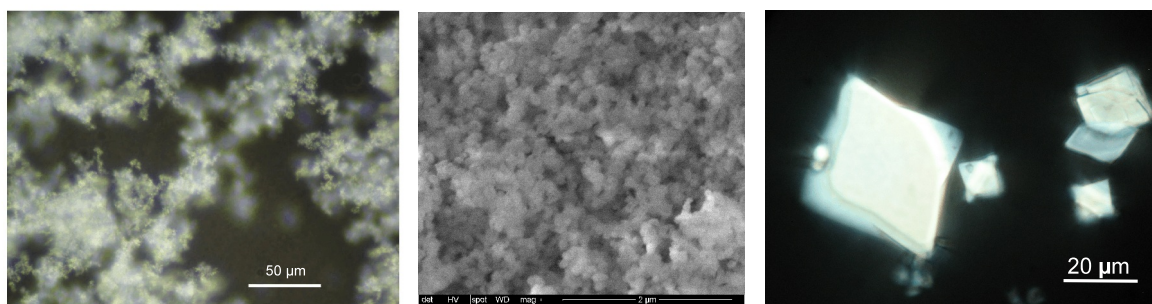

Figure 1. Strengite crystals from experiments without additive. Left: Dark-field image of precipitate from 30 mM solution of iron alum and ammonium dihydrogen phosphate. Center: SEM image of precipitate from 50 mM solution of either. Right: Circular polarization image of crystals formed from air oxidation of Fe(II) in phosphate solution.

X-ray diffractogram and Mössbauer spectrum are shown in Figures 2 and 3. The rather broad peak near 3 Å in the diffractogram agrees with four of the strongest reflections of strengite: 122, 221, 113 and 131. Similarly the Mössbauer spectrum agrees reasonably well with the findings of Dyar et al. on natural strengite from Minas Gerais in Brazil.[18] There is no agreement, on the other hand, with the dimorphic phase clinostrengite/phosphosiderite.
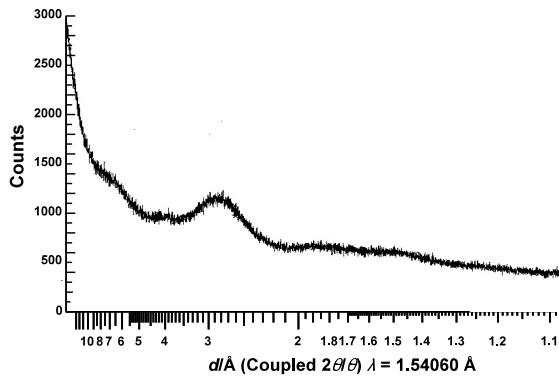
Figure 2. X-ray diffractogram of precipitate from iron alum and ammonium phosphate, typical of nanocrystalline strengite.
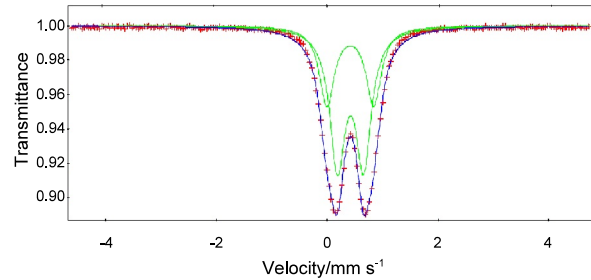
Figure 3. Mössbauer spectrum of precipitate from iron alum and ammonium phosphate.

Crystal growth of electrolytes from aqueous solution normally follows one or more of the classical kinetic expressions for spiral growth (Burton-Cabrera-Frank mechanism)

$$R_s = b\left(c_{Fe} - c_{Fe,eq}\right)\ln\beta \tag{2}$$

mononuclear growth

$$R_n = K_m S\left(\ln\beta\right)^{1/2}\exp\left[-\frac{4\lambda^2\bar{s}}{(kT)^2\ln\beta}\right] \tag{3}$$

or polynuclear growth (birth-and-spread mechanism)

$$R_n = K_p S^{1/3}\left(c_{Fe} - c_{Fe,eq}\right)^{2/3}\left(\ln\beta\right)^{1/6}\exp\left[-\frac{4\lambda^2\bar{s}}{3(kT)^2\ln\beta}\right] \tag{4}$$

In these expressions, which are simplified versions of a formalism originally proposed by Christoffersen et al,[19] b, K_m and K_p are rate constants, c_{Fe} and $c_{Fe,eq}$ are actual and equilibrium concentrations of iron, assumed to be rate-determining in surface processes, λ is edge free energy of a step on the crystal surface, $\bar{s}$ is the area occupied by a formula unit in the crystal surface layer, taken as the volume of a formula unit to the power of ⅔, and S is the average saturation ratio per ion constituent. The total saturation ratio, β, is defined as the ion activity product of the crystallizing substance divided by the corresponding solubility product; for strengite in the absence of additive we have

$$\beta = \frac{a\left(Fe^{3+}\right)a\left(PO_4^{3-}\right)}{K_{sp}(\text{strengite})} \tag{5}$$

where pK_{sp}(strengite) = 28.40.[13] Thus for strengite S equals the square root of β.

Polynuclear growth means that several surface nuclei are present and are growing at the same time on a crystal face, whereas in mononuclear growth there is only one nucleus per face. Both mechanisms show a dead zone at low supersaturation, where only spiral growth can be detected. Above this range growth accelerates, because nucleation may take place between the steps of a growth spiral, thus leading to a mixed growth law. The relation between the growth rates by spiral growth, R_s, by surface nucleation, R_n, and the overall growth rate R is expressed in Gilmer's equation[20]

$$\frac{R_n^3}{R^3} + \frac{R_s}{R} = 1 \tag{6}$$

Experimental data are now analyzed as follows: Growth rates are plotted against $(c_{Fe} - c_{Fe,eq})\ln \beta$ according to (2). If at low supersaturation the plot is linear and passes through the origin, it is concluded that the crystals grow by the spiral mechanism. The rate constant b is determined from the slope, and R_s may be calculated for the whole range of supersaturations studied. If the plot shows that growth accelerates at higher supersaturation, surface nucleation is likely to contribute. R_n as a function of supersaturation is then calculated using (6).

We now have two cases to consider: mononuclear growth according to (3) and polynuclear growth according to (4). To simplify expressions we shall use the following shorthand notations for the products between rate constant and exponential:

$$m(\beta) = S(\ln \beta)^{1/2}$$

$$p(\beta) = S^{1/3}\left(c_{Fe} - c_{Fe,eq}\right)^{2/3}(\ln \beta)^{1/6} \tag{7}$$

To test for surface nucleation and to determine λ we now plot either $\ln[R_n/m(\beta)]$ or $\ln[R_n/p(\beta)]$ against $1/\ln \beta$. If the plot is linear, a surface nucleation mechanism is confirmed, but we cannot directly from the plot tell whether it is the mononuclear or polynuclear mechanism due to the similarity of the expressions. However, the values found for λ will give a hint: for crystals with the structure and habit of strengite we should not expect widely different values for edge free energies of steps on different faces. This is what we should find, however, if we insisted on polynuclear growth as the only mechanism.

Figure 4 shows kinetic plots for precipitations from iron alum and phosphate, and Table 1 gives the values found for edge free energy as well as calculated initial values of pH and supersaturation.

With a small amount of precipitate, dissolved in hydrochloric acid, from one of the experiments with hydroxylamine additive, the usual Prussian-blue test was carried out. It was positive only for Fe(III), showing that oxidation was complete. In calculations on data from these experiments we have to make use of the reaction scheme given in the Introduction. We assume that the redox process is strictly connected with the crystallization process, which means that $[Fe^{3+}]$ is negligible in comparison with $[Fe^{2+}]$. The two acid dissociation constants of hydroxylamine are known from literature,[9,10] and so $[NH_3OH^+]$ may be calculated from solution composition like the concentrations of the other dissolved species. To calculate the crystallization affinity, which corresponds to supersaturation in the simple cases, we just need the equilibrium constant of the overall reaction, written here in the form of a solubility constant:

$$K'_{sp} = \frac{a\left(Fe^{2+}\right)^2 a\left(HPO_4^{2-}\right)^2 [NH_2OH]}{[NH_3]} \tag{8}$$
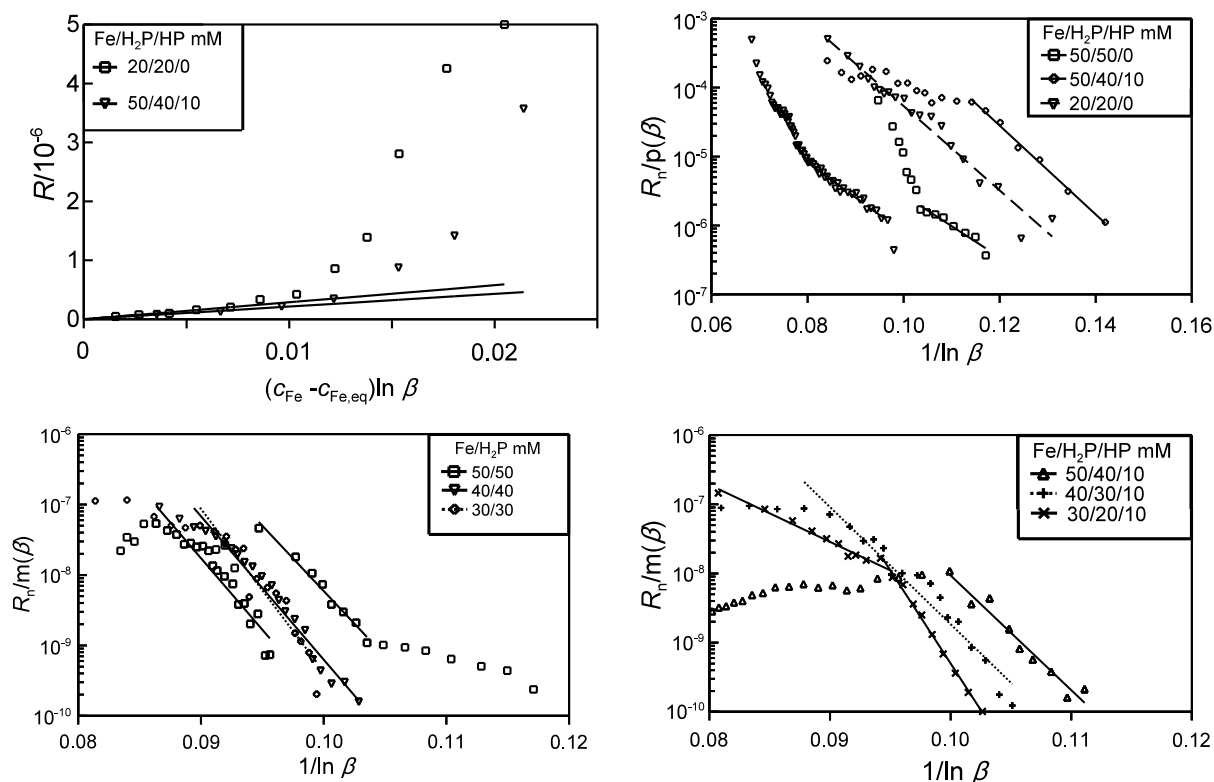
Figure 4. Crystal growth from iron alum and phosphate. Upper left: Spiral growth (BCF mechanism) at low supersaturation. Upper right: Polynuclear growth. Below: Mononuclear growth.

TABLE 1. Results for strengite crystal growth from solution of iron(III) and phosphate at 25°C.

$Fe/H_2PO_4^-/HPO_4^{2-}$, mM	pH_0	$\log \beta_0$	λ_m/pJ m^{-1}	λ_p/pJ m^{-1}
50/50/0	2.200	6.641	89±2	76±4
50/50/0	2.200	6.641	93±3	
40/40/0	2.235	6.596	96±2	
30/30/0	2.283	6.541	90±4	
20/20/0	2.355	6.468		81±1
20/20/0	2.355	6.468		89±2
50/40/10	2.332	6.819	84±4	
50/40/10	2.332	6.819		91±2
40/30/10	2.401	6.816	88±3	
30/20/10	2.510	6.837	58±2, 107±1	
Weighted mean			92±1	86±1

The value of this quantity may be calculated from the solubility product of strengite, the dissociation constants of the involved protolytes and the standard potentials of the iron and hydroxylamine couples. In this way we find at 25°C $pK_{sp}' = 48.47$. Using this value in kinetic analyses, however, we found unrealistic high values of surface and, in particular, edge free energies. Furthermore, the final pH recorded on the day after start of an experiment indicated that supersaturation was still very high without any sign of further reaction. Evidently a metastable state had been attained. It could be shown that this state obeys a law of constant ion activity product similar to that of a stable solubility equilibrium. The values of this parameter as calculated from final pH and used in kinetic analyses are

25°C: $pK_{sp} = 14.03 \pm 0.13$
35°C: $pK_{sp} = 14.40 \pm 0.13$

Kinetic plots on the basis of these values are shown in Figure 5, and edge free energies are given in Tables 2 and 3.
    The classical expression for homogeneous nucleation rate J per unit volume of solution as worked out by Becker, Döring, Volmer, Zel'dovich and Frenkel is

$$J = k_2 N_1^2 Z \exp\left[-\frac{16\pi\gamma^3\Omega^2}{3(kT)^3 \ln^2\beta} \right] \tag{9}$$

k_2 is a second-order rate constant for assembling of growth units, N_1 is the number density of single growth units in solution, and Z is the Zel'dovich factor accounting for the fact that the distribution of crystal embryos is not the equilibrium distribution. Different, but equivalent expressions for Z are found in the literature; one of them is[21]

$$Z = \frac{1}{8\pi\Omega}\left(\frac{kT}{\gamma}\right)^{3/2} \ln^2\beta \tag{10}$$

Further, γ is the surface free energy, and Ω is the volume of a formula unit in the crystal. As Z is proportional to $\ln^2\beta$, a plot of $\ln(J/\ln^2\beta)$ vs. $1/\ln^2\beta$ should have the same slope as that of $\ln(J/Z)$, and with this we find γ using (9).
    Determination of J from turbidity turned out to be rather difficult for pure systems with iron alum and phosphate. The dependence of number density on time became irregular a few seconds after start of the experiment, probably because of agglomeration and sedimentation. We could therefore make only a rough estimate of J from the first two or three points. Figure 6 shows the results. From the upper line we found $\gamma = 128 \pm 13$ mJ/m^2 and from the lower $\gamma = 120 \pm 40$ mJ/m^2, the weighted average being

$\gamma = 127 \pm 12$ mJ/m^2

For the systems with iron(II) and hydroxylamine the situation is quite different as Figure 7 shows. The rate of nucleation can be determined with rather high precision from the initial slope of a curve of particle number vs. time, and we get the rate of nucleation as function of supersaturation shown on the graph at right. The four leftmost points showing very precise linear dependence are assumed to represent homogeneous nucleation in accordance with Eq. (9), whereas the rest probably may

be ascribed to heterogeneous nucleation on unknown substrate. From the slope of the regression line we get
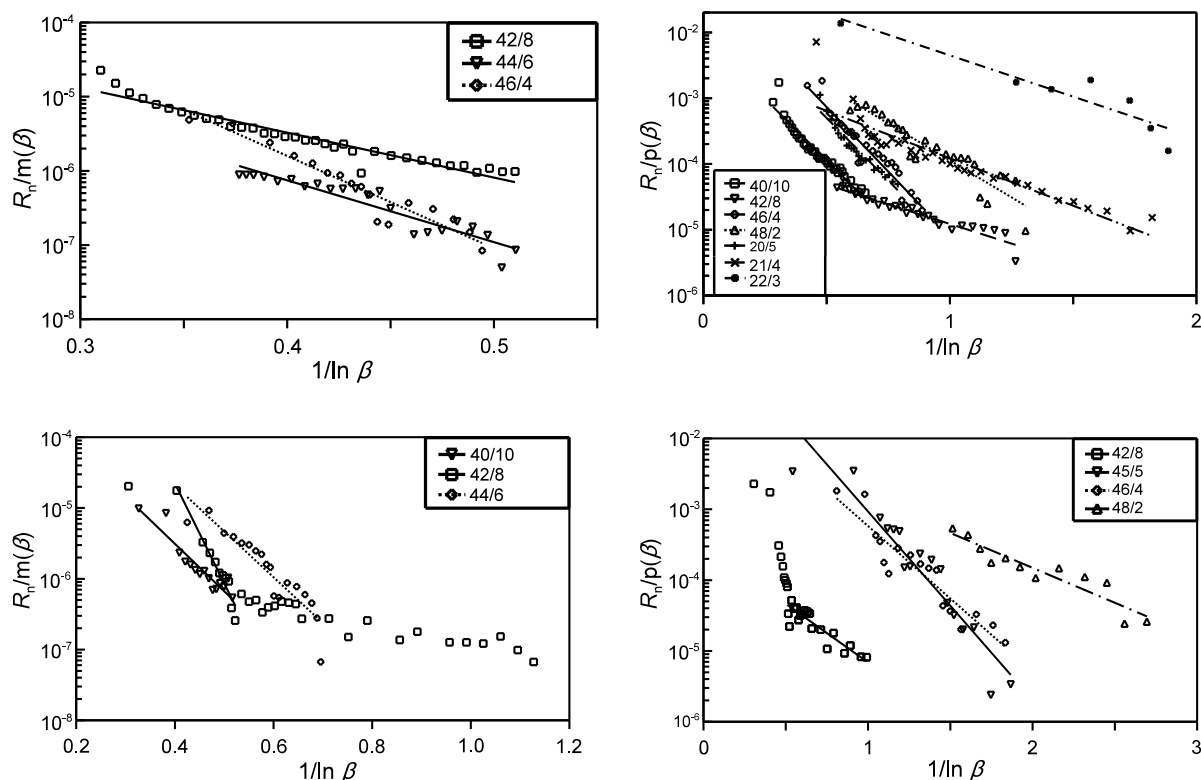
Figure 5. Crystal growth from iron(II), hydroxylamine and phosphate. Above: 25°C, below: 35°C. Left: mononuclear growth, right: polynuclear growth.

TABLE 2. Edge free energies λ (pJ/m) of strengite crystals grown at 25°C from solution of iron(II), phosphate and hydroxylamine. All solutions are 50 mM with respect to Fe(II).

| $H_2PO_4^-$, mM	HPO_4^{2-}, mM	mononuclear	polynuclear
40	10		20.8±0.4
42	8	16.1±0.4	12.4±0.4
44	6	18.9±0.8	
46	4	23.1±0.9	
46	4		22.4±0.6
48	2		17.0±0.7
20	5		22.1±0.6
21	4		13.6±0.5
22	3		12.7±1.1

TABLE 3. Edge free energies λ (pJ/m) of strengite crystals grown at 35°C from solution of iron(II), phosphate and hydroxylamine. All solutions are 50 mM with respect to Fe(II).

$H_2PO_4^-$, mM	HPO_4^{2-}, mM	mononuclear	polynuclear
40	10	17.5±0.9	
42	8	25.4±1.0	14.5±0.5
44	6	16.6±0.6	
45	5		20.0±0.8
46	4		16.7±0.8
48	2		11.6±0.7

$\gamma = 55.0\pm0.6$ mJ/m^2
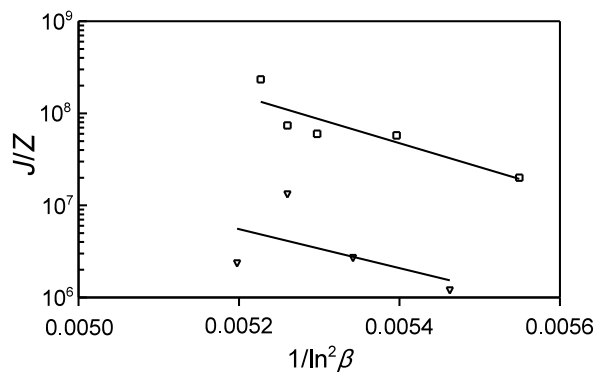
Figure 6. Approximate nucleation rates in solutions of iron alum and phosphate.
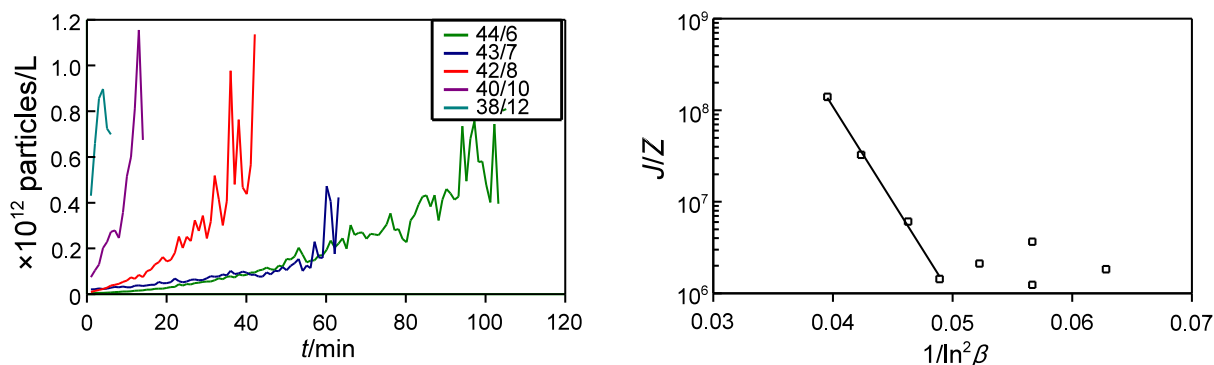
Figure 7. Results for nucleation kinetics of strengite crystallizing from solutions with Fe(II) and hydroxylamine. At left is shown the formation of new crystals as function of time at the 5 highest supersaturations. The right graph shows the rate of nucleation as function of supersaturation.
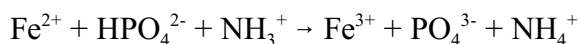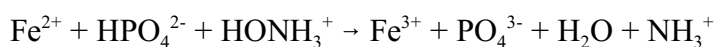
5. Discussion and conclusion

The above results of our study demonstrate not only the catalytic effect of growing iron phosphate crystals on the redox process involving hydroxylamine and leading to the crystallization of strengite rather than the expected vivianite. We also notice from the values in Tables 1-3 an important reduction in surface and edge free energies on crystals growing from solution with Fe(II) and hydroxylamine compared to those formed directly from Fe(III) and phosphate without additive. The high values found in the latter case, Table 1, are not unexpected for crystals of trivalent ions; this includes the not very precise surface energy determined from the plot of Figure 6. It is worth noting, however, that an alternative method of determining this quantity, based on critical supersaturation for nucleation, yields a similar result.[22] From the kinetic plots in Figure 4 we note that steady crystallization takes over, indicating that nucleation has ceased, somewhere in the range $0.08 \leq 1/\ln \beta \leq 0.10$; let us take the mean value, corresponding to $\beta = 6.7 \times 10^4$, as critical supersaturation for nucleation. When using Eq. (9) in this connection, the preexponential factor is often taken as $A = 10^{20}$ cm^{-3}s^{-1} for the lack of knowledge on the individual factors. Assuming further that at the critical supersaturation $J = 1$ cm^{-3}s^{-1}, we end up with $\gamma = 125$ mJ/m^2, i.e. the same value as that from turbidity within experimental error.

We further note from Table 1 that edge free energies are generally a little higher from mononuclear than from polynuclear growth. This may be understood if we realize that polynuclear growth is possible only if the crystal is sufficiently large to accommodate more than one growing surface nucleus per face; otherwise the mononuclear mechanism is the only possibility. Due to the long range of electrostatic forces the potential energy of a surface nucleus of a given size is lower on a large than on a small crystal, and this is registered as lowering of edge free energy.

In the case of crystallization from iron(II), hydroxylamine and phosphate we have three aspects to consider: 1) catalysis of the redox process by a growing crystal, 2) low values of surface and edge free energies, and 3) metastability of the final state, resembling an ordinary solubility equilibrium.

For the redox process a plausible mechanism could be the following: A surface layer with the composition FeHPO$_4$,xH$_2$O is formed on a strengite crystal. This is a likely assumption, as the concentration of HPO$_4^{2-}$ in the moderately acid solution is orders of magnitude higher than that of PO$_4^{3-}$, and deprotonation of the hydrogen phosphate ion is a rather slow process. A positive hydroxylammonium ion is now attracted to a negative phosphate site, where the following may take place, involving two neighboring sites:

$$Fe^{2+} + HPO_4^{2-} + HONH_3^+ \rightarrow Fe^{3+} + PO_4^{3-} + H_2O + NH_3^+$$

$$Fe^{2+} + HPO_4^{2-} + NH_3^+ \rightarrow Fe^{3+} + PO_4^{3-} + NH_4^+$$

The amidium ion formed in the first step is, of course, very unstable, so the second step is likely to be fast.

When looking at the values of edge free energy in Tables 2 and 3, we notice that they are even lower than those of vivianite[6] and fall in the range of a typical hydrated 2:2 salt like the calcium phosphate brushite, CaHPO$_4$,2H$_2$O.[23] In this connection it is worth noting that Füredi-Milhofer et al. found $\gamma = 50$ mJ/m^2 for this compound.[24,25] This supports the redox mechanism proposed above. The Prussian blue test does not rule out the presence of a monolayer of Fe(II), because the amount may be too small to be detected.

A certain influence of adsorbed hydroxylamine on surface and edge free energies cannot be

excluded either. Adsorption may be the cause of metastability as well, but in this connection it should be noticed that the major part of any crystal present is, in fact, strengite, the solubility of which determines the state of the system at the end of the process.

References

1 E S Dana, A Textbook of Mineralogy, 4th Ed. W E Ford (Ed.), Wiley, New York (1932) pp. 721, 723.

2 J O Nriagu and P B Moore, (Eds.), Phosphate Minerals, Springer, Berlin (1984) pp. 111f, 126f.

3 K Taxer and H Bartl, On the dimorphy between the variscite and clinovariscite group: redefined finestructural relationship of strengite and clinostrengite, $FePO_4 \cdot 2H_2O$, Cryst. Res. Technol. 39 (2004) 1080.

4 P Groth, Elemente der physikalischen und chemischen Krystallographie, Oldenbourg, München (1921) p. 176.

5 Standard Methods for the Examination of Water and Wastewater, 13th Ed., American Public Health Association, Washington, D.C. (1971) p. 190.

6 H E Lundager Madsen and H C Bruun Hansen, Kinetics of crystal growth of vivianite, $Fe_3(PO_4)_2 \cdot 8H_2O$, from solution at 25, 35 and 45°C, J. Cryst. Growth 401 (2014) 82.

7 J Emsley, The Elements, Clarendon, Oxford (1989) p. 128.

8 H E Lundager Madsen, Turbidimetric study of fluoride nucleation in solution, J. Colloid Interf. Sci. 307 (2007) 469.

9 R M Smith and A E Martell, Critical Stability Constants, Vol. 4: Inorganic Complexes, Plenum Press, New York (1976).

10 A E Martell, R M Smith and R J Motekaitis,Critically Selected Stability Constants of Metal Complexes, NIST Stand. Ref. Database 46, Ver. 5.0 (1998) and 8.0 (2004).

11 A K Grzybowski, The standard potential of the calomel electrode and its application in accurate physicochemical measurements. II. Thermodynamics of the second ionization of orthophosphoric acid, J. Phys. Chem. 62 (1958) 555.

12 N Bjerrum and A Unmack, Elektrometrische Messungen mit Wasserstoffelektroden in Mischungen von Säuren und Basen mit Salzen. Die Dissoziationskonstanten von Wasser, Phosphorsäure, Citronensäure und Glycin, Kgl. Dan. Vidensk. Selskab, Mat.-fys. Medd. 9(1) (1929) 143.

13 M Iuliano, L Ciavatta and G De Tommaso, On the solubility constant of strengite, Soil Sci. Soc. Am. J. 71 (2007) 1137.

14 H E Lundager Madsen, Aspects physicochimiques de la lithiase urinaire, Néphrologie 5 (1984) 161.

15 Y Berland, M Olmer, M Grandvuillemin, H E Lundager Madsen and R Boistelle, In vitro and clinical study of oxalate influence on calcium oxalate crystal formation, J. Cryst. Growth 87 (1988) 494.

16 G Mie, Beiträge zur Optik trüber Medien, speziell kolloidaler Metallösungen, Ann. Phys. 25 (1908) 377.

17 H C van de Hulst, Light Scattering by Small Particles, Wiley, New York (1957), Dover, New York (1981) chs. 9-10.

18 M D Dyar, E R Jawin, E Breves, G Marchand, M Nelms, M D Lane, S A Mertzman, D L Bish and J L Bishop, Mössbauer parameters of iron in phosphate minerals: Implications for interpretation of martian data, Am. Mineral. 99 (2014) 914.

19 J Christoffersen, M R Christoffersen and T Johansen, Some new aspects of surface nucleation applied to the growth and dissolution of fluorapatite and hydroxyapatite, J. Cryst. Growth 163 (1996) 304.

20 G H Gilmer, Growth on imperfect crystal faces: I. Monte-Carlo growth rates, J. Cryst. Growth 36 (1976) 15.

21 H E Lundager Madsen, Crystallization of heavy-metal phosphates in solution – III. Nucleation and growth kinetics of $Cd_5H_2(PO_4)_4,4H_2O$ at 37°C, J. Cryst. Growth 244 (2002) 349.

22 H E Lundager Madsen and C B Koch, Kinetics of solution growth of strengite, $FePO_4,2H_2O$, J. Cryst. Growth 482 (2018) 9.

23 S Rosa and H E Lundager Madsen, Influence of some foreign metal ions on crystal growth kinetics of brushite ($CaHPO_4·2H_2O$), J. Cryst. Growth 312 (2010) 2983.

24 H Füredi-Milhofer, M Marković, Lj Komunjer, B Purgarić and V Babić-Ivančić, Use of precipitation diagrams in determination of critical supersaturation for homogeneous nucleation, Croat. Chem. Acta 50 (1977) 139.

25 B Kosar-Grašić, B Purgarić and H Füredi-Milhofer, Precipitation of calcium phosphates from electrolyte solutions – IV. The precipitation diagram of calcium hydrogen phosphate, J. Inorg. Nucl. Chem. 40 (1978) 1877.